Discharge of vibrated granular silo: a grain scale approach

Arthur Pascot[a,*], Jean-Yves Morel[a], Sergiy Antonyuk[b], Mathieu Jenny[a], Yoann Cheny[a], Sébastien Kiesgen De Richter[a,c,*]

[a] *Université de Lorraine, CNRS, LEMTA, 2 Av. de la Forêt de Haye, F-54500 Vandœuvre-lès-Nancy, France*
[b] *Institute of Particle Process Engineering, University of Kaiserslautern, Gottlieb-Daimler-Str. 44/464, D-67663 Kaiserslautern, Germany*
[c] *Institut Universitaire de France (IUF)*

Abstract

The present work focuses on granular flows in a nearly-2D silo when external vibrations are applied. Experimental measurements and numerical simulations based on discrete element method (DEM) were performed in order to study the impact of both vibrations and opening size on the flow. Although vibrations make the flow possible for small opening sizes, we show that they can either increase or decrease the flow rate depending on the range of experimental parameters (amplitude, frequency, opening size...). The effect of vibrations amplitude (10-16000 µm) and frequency (15-75 Hz) on the flow was investigated. Two regimes are evidenced for the flow, governed by the Froude number Fr and the relative frequency Ω. In the first regime, vibration causes dead zones to flow and increases collision dissipation at the aperture while keeping the particle volume fraction constant. The flow rate decreases and can be described by Benyamine's law by introducing an effective velocity that accounts for the effect of vibrations on the fall of particles at the outlet. In the second regime, the perturbations due to vibrations then surpass the gravity driven flow, leading to periodic shocks in the silo and increasing the apparent flow rate.

Keywords: `Hopper flow, Granular material, Vibrations, Rheology`

1. Introduction

Granular materials are the most widely used matter in industries after water, though also far more complex. Contrary to colloids for example, granular materials are by their size most often non-Brownian and therefore not subject to thermal agitation. This can lead to blockages of the flows on the different processing lines of these materials. Mechanical vibrations appear then as an alternative widely used to homogenize the material in industrial processes, such as in the controlled feeding of dry bulk materials, the screening

*Corresponding author
Email addresses: `arthur.pascot@univ-lorraine.fr` (Arthur Pascot), `sebastien.kiesgen@univ-lorraine.fr` (Sébastien Kiesgen De Richter)

of dry and wet products, the transport of large tonnages of bulk materials or for vibrating bins, bowls and hoppers. An important result of the last few years has shown that applying controlled mechanical vibrations to a granular assembly gives it remarkable properties to control its viscosity by removing the apparent yield stress of the material [1, 2, 3, 4]. It seems clear in the literature that vibrations break chains of forces and allow the flow rate to be controlled [5, 6, 7, 8], but questions remain about the mechanisms that take place at the particle scale and in particular about how vibrations modify their dynamics and collective motion. This is a relatively complex problem because vibrations are generally transmitted through the walls and partly dissipated by contacts between grains. To investigate the effect of vibrations on particle dynamics, we present here a study in a very simplified configuration consisting of a quasi 2D vibrating silo.

The flow in granular silos has been extensively studied, starting with Beverloo et al. [9]. The authors have shown that the flow rate mostly depends on the opening size and particle properties while proposing an empirical law linking them. More recent studies have evidenced limits to this law, in particular when the opening size tends to the particle diameter [10, 11, 12] and for more complex flows [13, 14] with non spherical or poly-disperse particles. Different corrections have been proposed to predict the flow rate in those cases, generally by taking into account the decrease of volume fraction at the opening due to particle-particle collisions [10, 11, 12]. However, those laws fail to predict both the clogging of the silo due to the formation of arches at the opening and the flow rate when vibrations are applied to avoid arches formation [15, 16, 17, 18]. Despite a few studies on the subject [19, 20], questions remains regarding the impact of vibrations on the rheology of granular flows in vibrated silos and, more precisely, on how vibrations modify the dynamics of the particles in such a configuration.

In our previous work [21, 22], the flow rate during the discharge of monodisperse glass beads in a quasi-2D silo under vertical vibrations was studied. This geometry has the advantage of revealing dead zones where the flow is blocked in the absence of vibrations, and it also allows us to follow the movement of the particles with a high degree of accuracy. A better understanding of the effect of vibrations on particle dynamics in such a simple geometry is a first step before attempting to model the behaviour in vibrated 3D silos for granular media of various compositions. In the study, two regimes were evidenced for the flow rate and an empirical law was proposed to describe them depending on the vibrations and silo geometry. Those results allow an useful macroscopic description of the discharge but questions remain on the mechanisms involved at the grain scale, in particular on how the volume fraction and velocity of the grains are changed by vibration at the outlet.

In this paper, we present experimental and numerical results for a better understanding of the influence

of vibrations on the flow at the grain scale during the discharge. Numerical simulations are used to analyse the behaviour at very high vibration intensities which are difficult to achieve experimentally in a controlled manner. In Sec. 2, the experimental setup and numerical model used are presented. In Sec. 3, the measured mean flow rate is linked to particles dynamics at the outlet. In the last part, we discuss the fluctuations of the velocity profiles during a period of vibrations and relate it to the competition between gravity driven and vibrations driven reorganisations at the particle scale.

2. Methods

2.1. Experimental setup

The experimental setup used (see fig. 1a and b) is composed of a rectangular transparent silo ($H = 300$ mm, $L = 100$ mm) mounted on a vertical shaker. The opening size D of the silo can be freely changed to fit different configurations (see table 1). Similarly to our previous setup [21, 22] and other studies [11, 16, 18], the silo is quasi-2D with a depth $W = 1.5$ mm, which allows the flow of only one layer of particles. This configuration allows a 2D flow which can be recorded with a camera and prevents wall effects in the other directions. To avoid static electricity during the discharge, the silo is made of anti-static PMMA and an anti-static coating is also applied regularly.

Figure 1

The particles used are non-cohesive spherical glass beads (Silibeads type S) with a diameter $d = 1.1 \pm 0.1$ mm. These particles are collected in a container using a hopper on an articulated arm. The container is placed on a dynamic scale which measures the macroscopic mass flow rate Q. The shaker applies vertical and sinusoidal vibrations, whose amplitude A and frequency f can be finely tuned. Due to the mass of the silo (3 kg), the shaker is limited to 108 m/s^2 for the acceleration. Thus, vibrations can be applied up to a maximum relative acceleration $\Gamma = A\omega^2/g = 11$, where g is the gravitational acceleration and $\omega = 2\pi f$ the pulsation. This is the main change compared to the previous setup [21], which could only reach $\Gamma = 3.3$.

Table 1

Lastly, a CCD camera record a 10 by 10 cm area above the opening to at least 1000 images per second with a image resolution of 10 pixels/mm (see recorded area in fig. 1a). An inclined LED panel behind the setup is used to illuminate the flow (see fig. 1b).

2.2. Numerical model

To achieve high vibration accelerations ($\Gamma > 11$), discrete element simulations (DEM) are also performed using the open-source software LIGGGHTS [23, 24]. This software is an extension of LAMMPS (widely used in molecular dynamic) based on the work of Cundall and Strack [25] to simulate the mechanical behaviour of each particle in a granular assembly. The geometry of the silo (created and meshed using the open-source software FreeCAD) is the same as the one used in experiment. As in experiment, non-cohesive spherical glass beads of diameter $d = 1.1 \pm 0.1$ mm are inserted[1] in the silo and then discharged while vertical and sinusoidal vibrations are applied. The only difference with the experiment is the limit for the vibrations, which was fixed at $\Gamma = 30$ in simulation. Above this limit, the flow becomes highly unsteady while a transition to a granular gas is observed due to the extreme values of vibrations. A snapshot of the simulated silo during a discharge is presented in fig. 1c. Similarly to the scale in experiment, a zone bellow the silo outlet counts the exiting particles to measure the mass flow rate Q.

In the simulation, the position, velocity and forces on each particle are calculated and updated with a constant time-step $\Delta t = 1 \times 10^{-5}$ s. The particle are inserted (for 2 s) in the silo and then vibrated (for 0.5 s) before opening the silo to start the discharge and capture the stationary (or quasi-stationary) flow regime (for 2.5 s). The contacts between particles and walls are resolved using a *soft sphere approach* (Young modulus $E < 1 \times 10^9$ Pa) and the *Hertz contact model* developed by Di-Renzo et al. [26]. The physical properties used are based on the literature and calibrated on the experiment without vibration (see table 2). The soft sphere approach and constant friction coefficients μ used allow a minimization of the simulation time[2] while giving realistic estimations of the flow rate and flow pattern in the silo [21].

Table 2

2.3. Flow analysis

To study the flow during the discharge, the position and velocity of the particles are recorded in both experiment and simulation. In simulation, all information can be directly extracted and stored. In experiment, the particle centers appear as bright spots on the images from the camera (see fig. 2). Those spots can be detected and tracked to obtain the trajectory of each particle, and thus their position and velocity. The detection and tracking are performed with the software Matlab, using functions developed by Daniel Blair

[1] Particles are generated at the top part of the silo using a random seed and then fall, filling up the silo.
[2] Typical CPU time is 50 min per simulation using an 8 cores Intel Xeon Processor E5.

and Eric Dufresne[3], adapted from the free software "Particle tracking using IDL"[4] of John C. Crocker and Eric R. Weeks [27]. This program has the advantage of allowing to follow a very large number of particles and to measure displacements with a sub-pixel resolution (1/10 pixel precision). In our case, about 10 000 particles are captured at each time with an image resolution of 10 pixel/mm (i.e. 10 µm precision for particle position with the sub-pixel detection).

In the following, the positions and velocities are always given in the referential of the silo (see fig. 2). The movement of the silo due to the vibrations is thus subtracted from the movement of the particle:

$$\mathbf{x}_p^{ref} = \mathbf{x}_p^{abs} - \mathbf{x}_{silo}^{abs} = \mathbf{x}_p^{abs} - A\sin(\omega t).\mathbf{e_z} \tag{1}$$

$$\mathbf{v}_p^{ref} = \mathbf{v}_p^{abs} - \mathbf{v}_{silo}^{abs} = \mathbf{v}_p^{abs} - A\omega\cos(\omega t).\mathbf{e_z} \tag{2}$$

where t is time, $\mathbf{x} = (x, z)$ and $\mathbf{v} = (v_x, v_z)$ are the position and the velocity of particles respectively. The subscript p and $silo$ refer to the particle and silo respectively. The exponent ref and abs are respectively related to the referential of the silo and the lab.

Figure 2

In this work, we focus on the flow at the opening of the silo in the steady (or quasi-steady) flow regime. In this regime, the mass flow rate is constant on a macroscopic time scale (~ 1 s) due to the pressure saturation in the silo [9] (temporal fluctuations can however still be observed, in particular when adding vibrations). The beginning and end of the discharge where unsteady effects take place are excluded from this work.

Using the information from the particles, the velocity $\mathbf{v}$ and volume fraction ϕ were calculated in the semi-circle of radius $r_0 = D/2$ just above the silo opening (see "outlet" in fig. 2). The flow in this area tends to a free fall motion as shown by recent studies [10, 12, 28, 29]. A volume average is performed from the information of the particles in the outlet to calculate the mean value of each quantity (more details in Appendix). The mean velocity and the mean volume fraction are characteristic of the magnitude of the silo outflow and can be used to calculate the mass flow rate of the silo.

In addition to those spatial averaged quantities, the inflow profiles surrounding the outlet area are also measured. To avoid discrete effects due to particle size, those radial profiles are measured along a radius

[3]Basic principle of the tracking: a function is first used to search in the frames recorded for bright blob of pixels with a user-defined radius and brightness. Once detected, the position of the particles are stored for each frame. A tracking function is then used to link the position of the particles between two consecutive frames by determining the most probable displacement within a maximum range provided by the user. Functions and more information available at: https://site.physics.georgetown.edu/matlab/

[4]Software available at: http://www.physics.emory.edu/faculty/weeks//idl/

$r_1 = D/2 + d$ (see "profile" in fig. 2) and have a thickness $2d$ ($r = r_0$ to $r_0 + 2d$). For those profiles, the inflow depends on the radial velocity v_r defined as:

$$v_r = v_x \cos(\varphi) + v_z \sin(\varphi) \tag{3}$$

where v_x and v_z are the velocities along axis x and z, while φ is the angle of the radial position. A weighted average is performed from the information of the particles close to each point of the profile ($distance \leq d$) to calculate the mean profile for each quantity (more details in Appendix). Those profiles of velocity and volume fraction are characteristic of the shape of the silo outflow and can be related on the flow inside the rest of the silo.

3. Results

3.1. Macroscopic flow rate and regimes

The influence of opening sizes $D = 5 - 20$ mm, frequencies $f = 15 - 75$ Hz and amplitudes of vibration $A = 0 - 2800$ µm were studied using the experimental set-up described in the previous section. Adding vibrations make appear two distinct regimes for the normalized flow rate Q/Q_0 (where Q_0 is the flow rate without vibration), as previously discussed in [21] and presented in fig. 3a and b. Each regime depends on the vibration amplitude A as well as the opening size D (fig. 3a) and vibration frequency f (fig. 3b). Note that each point in fig. 3a and b is an average over 3 independent measurements of the mean flow rate in simulation and experiment during the stationary discharge. While the flow rate is constant at the macroscopic scale (~ 1 second), temporal fluctuations are observed without vibration and in each regime as presented in fig. 3c . In each case, typical mean velocity fields $|\mathbf{v}|$ in the silo which differ from the case without vibration are presented in fig. 4.

Figure 3

Figure 4

Figure 5

In the first regime, the flow rate decreases when increasing the vibrations, as previously reported by Wassgren et al. [20] for a different silo geometry. In this regime, the vibrations allow the dead zones to flow which increases the competitiveness at the opening and induces more contacts between particles [30]. This leads to a transition from a funnel flow without vibration to a mass flow (see fig. 4). As shown in the insert of fig. 5a, the decrease of flow rate depends on both the amplitude A, the frequency f of the vibration

and the size of the opening D. The DEM results well capture the existence of this flow drop in this first regime induced by vibrations. All the data can be well rationalised (see fig. 5a) by introducing the Froude number $Fr = A\omega/\sqrt{gD}$, defined as the ratio between the characteristic velocities induced by the vibration and gravity. In this first regime, as proposed in [21] the flow rate Q can be well fitted to an empirical exponential law $\mathcal{F}_1$ such that:

$$\frac{Q}{Q_0} = 1 + \mathcal{F}_1 \tag{4}$$

$$\text{with:} \quad \mathcal{F}_1 = -a_1 \exp(-b_1/Fr) \tag{5}$$

where Q_0 is the flow rate without vibration, a_1 and b_1 are two adjustable parameters.

In the second regime, the flow rate increases when increasing the vibrations (see fig. 3). This regime is due to the propagation of shock waves [21, 22] in the silo, as observed for vibrated granular heaps [31, 32]. Those waves are created by the propagation of the vibration in the silo and the fall of the particles due to gravity. This dynamics acts as a piston periodically compressing the particles above the opening [21, 22]. This leads to periodic high bursts of flow rate (when the silo goes up while the particles fall down), with nearly no flow in-between as observed for the instantaneous flow rate in fig 3c. In this regime, the dead zones continue to flow while the velocity in the funnel greatly increases (see fig. 4). To isolate this second regime, we remove the contribution of the first regime by plotting $\mathcal{F}_2$ as a function of Fr (see insert in fig. 5b):

$$\mathcal{F}_2 = \frac{Q}{Q_0} - (1 + \mathcal{F}_1) \tag{6}$$

The increase of flow rate not only scales with the Froude number Fr but depends on the square root of the relative frequency $\Omega = \omega/\sqrt{g/d}$ (see fig. 5b), where d is the particle diameter. This relative frequency can be seen as a ratio between the typical time for a particle to fall from a diameter due to gravity and the period of the vibration. It reflects the phase shift between the oscillating movement of the silo and that of the particles [21, 22]. The flow rate is then controlled by the competition between the typical power injected by the vibrations, $\mathcal{P}_{vib} \propto A^2 f^3$ and the typical power of gravity forces $\mathcal{P}_{grav} \propto g^{3/2} d^{-1/2} D$ at the outlet. Note that this behavior is well captured by the simulations (see fig. 5a and b), though the second regime increases slightly more sharply than in experiment. This comes from more complex friction between particles (friction coefficients are imposed constant in simulation and calibrated in the case without vibration and in the first regime) and a slight damping (in-homogeneity and resonance) in the experiment due to the extreme vibrations applied ($\Gamma \sim 10$). Despite this difference, the simulation allow us to extrapolate the behavior for

high intensity, confirming the increase observed in experiment but also showing the beginning of a saturation for extreme vibration. It is also worth noting that all the data can be well fitted to an empirical law very similar to the one proposed for F_1 such that (see [21, 22]):

$$\mathcal{F}_2 = a_2 \exp\left(-b_2/(Fr\Omega^{1/2})\right) \tag{7}$$

where a_2 and b_2 are two adjustable parameters.

From those results, the influence of vibrations on the flow rate can be well described by the function:

$$\frac{Q}{Q_0} = 1 + \mathcal{F}_1 + \mathcal{F}_2 \tag{8}$$

where $\mathcal{F}_1$ and $\mathcal{F}_2$ describe the flow in the first and second regime respectively. Those results and the macroscopic law proposed remains however empirical and in the next section we will discuss the microscopic origin of the observed two regimes at the particle scale.

3.2. Grains motion at the outlet

To better understand the origin of the two regimes and the empirical law, the flow at the opening of the silo was studied for different opening sizes D and amplitudes A ($f = 30$ Hz) in experiment and simulation. The velocity v and volume fraction ϕ were measured, either in the semicircle at the outlet or along the profile surrounding it, as described in Sec. 2.3 (see fig. 2).

3.2.1. Time-averaged profiles at the opening

The velocity and volume fraction are first averaged over 2 seconds in the stationary discharge to obtain the time-averaged values and profiles near the opening. The radial velocity v_r and volume fraction ϕ are measured along the profile surrounding the outlet (in green in fig. 2), as presented in fig. 6.

Figure 6

Without vibration, a Gaussian velocity profile is observed (black line in fig. 6a,b,c) in agreement with the kinematic model[5] used in the literature for silo discharge [33, 34, 35]. Increasing the amplitude leads to a flattening of the profiles: the flow slows down in the flow channel ($\varphi \approx \pi/2$) while grains in the dead zones on the side are put in motion ($\varphi \approx 0$ and π). This behavior is perfectly consistent with the transition to a mass

[5]The velocity v_r without vibration is fitted to the following equation: $v_r = a\exp(-b(\varphi - \pi/2)^2) + c$. This equation describes a Gaussian curve with an offset, which is an approximation at the outlet of the kinematic model [33, 34, 35].

flow observed previously in the silo (see fig. 4). In the second regime, the outflow velocity increases around the silo opening. This is due to the shock dynamic acting as a "piston" propelling the particles outside of the silo. This behavior is particularly apparent for the smallest opening size $D = 5.26$ due to the higher Froude number reached, in accord with the two scaling for the flow rate (see Sec. 3.1).

Conversely to the velocity, the volume fraction (fig. 6d,e,f) remains nearly constant for all the amplitudes. This implies that the evolution of the flow rate Q when vibrations are applied is directly related to the change of the velocity profile at the opening, and not related to a significant change of volume fraction (contrary to the case without vibration as reported in the literature [11, 12]). Considering this result, the law proposed by Benyamine et al. [12] for 2D silo can be generalized to the vibrating case. The mass flow rate without vibration is given by:

$$Q_0 = \rho\phi_0 W D \times \mathcal{V}_0 \tag{9}$$

where ϕ_0 is the volume fraction at the outlet. In that case, $\mathcal{V}_0$ equals $C\sqrt{gD}$ where C is a constant, which corresponds to an effective outflow velocity at the opening. From this equation and eq. 8, we obtain for the vibrating case:

$$Q = Q_0(1 + \mathcal{F}_1 + \mathcal{F}_2) = \rho\phi_0 W D \times \mathcal{V}_0(1 + \mathcal{F}_1 + \mathcal{F}_2) \tag{10}$$

which can be expressed as:

$$Q = \rho\phi_0 W D \mathcal{V}_{vib} \quad \text{with:} \quad \mathcal{V}_{vib} = \mathcal{V}_0(1 + \mathcal{F}_1 + \mathcal{F}_2) \tag{11}$$

where $\mathcal{V}_{vib}$ is the effective outflow velocity induced by both gravity and the vibration.

3.2.2. Evolution of the profiles during the discharge

In the previous section, the mean flow was obtained by integration of the time averaged velocity profiles, but transient phenomena also appear at the time scale of the vibration period. In particular, a frequency response to the vibration is observed for the flow rate (see fig. 3c). These transient phenomena cause a reorganisation of the particles and an unsteady evolution of the velocity during the vibration period. Thus, to understand those phenomena, the radial velocity v_r and volume fraction ϕ profiles were measured at different time $t \in [0 - T]$ during a vibration period $T = 1/f$. For each time[6] t, profiles are ensemble averaged over 60 cycles of vibration to isolate the periodic behavior while suppressing random fluctuations. The

[6]The instants $t = 0$ and $t = T$ were only averaged over 30 periods of vibrations (e.g. $t = 0, 2T, 4T...$ and $t = T, 3T, 5T...$) to avoid overlapping.

characteristic profiles, the height z_{silo} and the vertical velocity $v_{z,silo}$ of the silo during a period of vibration are presented in fig. 7.

Figure 7

As observed for the flow rate, adding vibrations in the first regime leads to periodic fluctuations during the discharge (fig. 7a and c). These fluctuations are periodically positive and negative due to the direction of the vibration, resulting in different transient velocity profiles (see fig. 7a) related to the silo motion: higher outlet velocities as the silo begins to rise ($t \in [3T/2 - T]$) and lower velocity as it falls ($t \in [T/4 - T/2]$). Similarly to the mean profiles (see Sec. 3.2.1), the vibrations mostly affect the instantaneous outlet velocity keeping the volume fraction constant.

In the second regime, the radial velocity profiles during a period of vibration (fig. 7b) oscillates between high negative values during the burst dynamics ($t \in [3T/4 - T]$, when the silo starts to go up while the particles fall down) to positive values for the highest vibrations ($t \in [T/4 - T/2]$ when the silo is at its top position and begins to fall down while the particles continue to rise or to fall down with a lower velocity)[7]. Before each burst ($t = T/2$ in fig. 7d), compression is observed on the profiles of volume fraction ϕ. This compression comes from the shock propagating in the silo, as observed in our previous study [22].

3.2.3. Statistical and frequency analysis at the outlet

The evolution of the velocity and volume fraction profiles with time provide us information about the effects of the vibrations on the time scale of the period. To better quantify those effects, the velocity v_z and volume fraction ϕ at the outlet during the discharge were also measured over 2 seconds. The time evolution, statistical distributions (Probability Density Function) and Fourier analysis obtained for different amplitudes $A = 0 - 2800$ µm ($f = 30$ Hz, $D = 5.26$ mm) are presented in fig. 8.

Figure 8

Without vibration, the velocity and volume fraction are nearly constant over time as shown by the flat time signals and the tight peaks of probability density function around the mean values.

Adding vibrations in the first regime ($A = 500 - 800$ µm) creates periodic fluctuations with the same frequency as the vibrations, resulting in an enlargement of the PDFs. In particular, two peaks are observed for the velocity at $v_0 - \delta$ and $v_0 + \delta$, with v_0 the mean velocity without vibration and δ a small perturbation. In this regime, gravity is the main driving force leading to a stable state (v_0) while vibrations induce small

[7] It should be noted that there is always a delay between the vibration of the silo and the movement of the particles due to conservation of momentum for the particles

perturbations around this state ($\pm\delta$). For the volume fraction, both the higher fluctuations and enlargement of the PDF reflect breakage of the contacts between particles. Those reorganisations cause dead zones to flow and increase the number of collisions. This results in higher energy dissipation due to collisions and therefore a lower average flow rate [21, 30]. Those velocity and volume fraction fluctuations lead to an harmonic response of the system, as shown by the response at the frequency of the vibration f. The response amplitude increases with the Froude number Fr, which accounts for the competition between the effect of vibrations and gravity.

In the second regime ($A = 1400 - 2800$ µm), velocity v_z and volume fraction ϕ variations have a wider range of values than those in the first regime. Periodic oscillations between two extreme values are observed for the two quantities with the same frequency as the vibration. This is caused by the burst dynamics induced by the vibration at large amplitude A (see Sec. 3.1). The peaks of negative velocity and maximum volume fraction correspond to the periodic burst of flow rate ("burst" in fig. 8). Conversely, the peaks of positive velocity and minimum volume fraction correspond to the periods between burst with nearly no outflow ("no flow" in fig. 8). Those two behaviors are also observed in the PDFs, which are greatly enlarged and present two local peaks for the burst and periods of "no flow". The periods of "no flow" correspond to a counter flow opposed to gravity when the silo goes up. Despite this counter flow, a shift of the velocity distribution (fig. 8b) towards the negative values is observed when increasing the vibration, which denotes the increase of flow rate in the second regime. In this regime, the vibration are the main driving force of the discharge, creating perturbations greatly surpassing the gravity and causing the shock dynamics. Accordingly, we observe a sharp increase of the response amplitude for the velocity at the vibration frequency f (see fig. 8c), compared to the mean response ($f_a = 0$ Hz). Smaller peaks at harmonic of f (60, 90, 120 Hz) are also observed in this regime. They are caused by the propagation of the waves in the higher part of the silo [21, 22], leading to secondary shocks (the main ones happening just above the opening at the frequency of the vibration).

Figure 9

To better quantify the contribution of velocity fluctuations observed on the flow rate, the mean response $v_{z,0Hz}$ (peak at $f_a = 0$ Hz in fig. 8c) and response at the frequency of the vibration $v_{z,30Hz}$ (peak at $f_a = f$) are measured in both experiments and DEM simulations. As discussed in 3.1 for the flow rate, the effect of the vibration are well captured by the simulation (though with slight quantitative differences), which also confirm the frequency response in the second regime. The evolution with the Froude number of the normalized quantities $v_{z,0Hz}/v_0$ (see fig. 9a) and $v_{z,30Hz}/v_0$ (see fig. 9b), where v_0 is the mean velocity without vibration, are calculated in both experiment and simulation. The zero-frequency response $v_{z,0Hz}/v_0$ perfectly fits the

law for the flow rate (eq. 8, see fig. 6), whereas $v_{z,30Hz}/v_0$ continuously increases with the Froude number and can be well fitted to a simple logarithmic law:

$$\frac{v_{z,30Hz}}{v_0} = \alpha \ln(Fr + 1) \tag{12}$$

with $\alpha = 1.89$ a fitting coefficient. We observe that the the transition between the two regimes verifies[8] $v_{z,30Hz}/v_0 = 1$. Vibrations induce small perturbations of the gravity-driven flow in the first regime ($v_{z,30Hz} < v_0$) but become predominant in the second regime ($v_{z,30Hz} > v_0$). The logarithmic behaviour indicates a decreasing efficiency of the response of individual particles to vibrations. This is due to a transition from a regime where each particle oscillates in cages formed by its neighbours (the first regime) to a collective motion where the whole packing oscillates during the shock dynamics (the second regime). It is important to notice that both mechanisms coexist for all the range of Froude numbers studied here but one dominates in each regime depending on the intensity of the vibrations.

4. Conclusions

In this paper, we study the discharge of model granular materials inside a quasi-2D silo under vibrations. Although vibrations are most often used to improve the flowability in granular media applications, we show for the first time on a model 2D silo configuration that counter-intuitive behaviours can occur: vibrations tend to decrease the apparent flow rate or drastically increase it depending on their intensity.

Experiments and numerical simulations are performed to better understand the origin of the two regimes observed for the flow rate [21]. The velocity profiles at the outlet of the the silo are measured and discussed. The variations of the flow rate is directly proportional to the variation of the velocity at the outlet, the volume fraction keeping nearly constant. Without vibration, a steady state is reached, with a constant velocity due to gravity. Adding vibrations leads to velocity fluctuations around this state. Those fluctuations are periodic with the same frequency as the vibrations and increase with the Froude number Fr.

In the first regime, velocity fluctuations are small compared to the mean velocity of the flow induced by gravity. This leads to a stationary regime primarily driven by gravity, with sinusoidal slight perturbations around the average state. The vibrations allow the particles located in the dead zones to move, leading to a more homogeneous but slower flow. The slowdown comes from an increase of the number of contacts in the funnel due to the fluctuations (longer distance travelled by the particles) and an increase of competitiveness

[8] In our case, the transition occurs for $Fr = e^{1/\alpha} - 1 = 0.70$. Note that the relative frequency Ω should also be taken into account.

at the outlet.

In the second regime, velocity fluctuations are larger than the mean velocity induced by gravity. The discharge rate is then driven by the vibrations, with an intermittent flow oscillating between large bursts and nearly no flow. This is due to the propagation of the vibrations waves in the silo, leading to shock above the opening. Those shocks compress the particles and push them out as periodic dense bursts when the silo goes up. Outside of those burst, the particles tend to either follow the movement of the silo or even go up, thus resulting in a near zero flow rate.

The flow rate in a quasi-2D silo under vibration can then be modelled by the following empirical law:

$$Q = \rho\phi_0 W D\mathcal{V}_{vib} \quad \text{with:} \quad \mathcal{V}_{vib} = C\sqrt{gD}(1 + \mathcal{F}_1 + \mathcal{F}_2) \tag{13}$$

where $\mathcal{V}_{vib}$ is the effective outflow velocity when vibrations are applied.

Those results give a better understanding of the physical mechanisms behind the two regimes and empirical law for the flow rate. Still, further studies are required to completely describe the flow inside the entire silo. With this aim on mind, particular care should be taken regarding the temporal aspect of the flow. On a macroscopic scale, a time averaged approach works well to describe the flow under vibration as seen here. However, an unsteady model may be needed to describe the flow accurately at the microscopic scale. This is particularly the case for the second regime which is strongly time dependent. It also should be mentioned that those results were obtained in an "ideal" case (spherical and non cohesive particles). Extending them to more complex, in particular cohesive particles, is another important prospect given the use of granular silo in industries. Although applied to a model 2D geometry, this study shows that the addition of vibrations can increase or decrease the flow rate depending on the range of vibrations parameters studied. Our results and the mechanisms involved suggest that there is no reason why this type of behaviour should not also be observable in 3D. In particular, it can be useful for fine control of flows on industrial lines and on how to optimize vibration control on processing lines according to the desired flow rate.

Acknowledgements

We acknowledge support from the Agence Nationale de la Recherche/DFG (Project "pastflow" ANR-19-CE08-0030-01). A part of this study is conducted in the framework of the "PowderReg" project, funded by the European programme Interreg VA GR within the priority axis 4 "Strengthen the competitiveness and the attractiveness of the Grande Région / Groβregion

Appendix

During the discharge of the silo, position and velocity of the particles were measured at each time in experiment and simulation. This information was then used to calculate the velocity and volume fraction at the outlet and along the surrounding radial profile (see fig. 2). To obtain precise results, particular care should be taken regarding the discrete aspect of the flow due to particle size [36, 37]. Thus, different methods were used to calculate the volume fraction and the spatial averages at the outlet and along the profile:

Figure A.1

Calculation of the volume fraction: by definition, the volume fraction for an assembly of particle is given by:

$$\phi = \frac{\sum_{k=1}^{n} V_k}{V_t} \tag{A.1}$$

with n the number of particles, V_k the volume of the particle k and V_t the total volume of the assembly. However, this definition is only relevant for a sufficiently large number of particles. For a few particles ($n \to 1$), this definition will lead to extremely variable results. To avoid this problem and obtain a representative volume fraction even at the scale of the particle, we instead calculate the *free volume* V_{free} around each particle. This volume denotes the space available to a particle to move between its neighbours and can be calculated using a *Voronoi tessellation*[9] [38]. In our case, we use a 2D Voronoi tessellation (see fig. A.1a) and the free volume for a particle k is given by:

$$V_{free,k} = V_{vor,k} - V_k = A_{vor,k} W - V_k \tag{A.2}$$

with $V_{vor,k}$ and $A_{vor,k}$ respectively the volume and area belonging to the particle given by the Voronoi tessellation and W the depth of the silo. Using this free volume definition, a local volume fraction can be deduced for any number of particles:

$$\phi = \frac{\langle V_k \rangle}{\langle V_{free,k} \rangle + \langle V_k \rangle} \tag{A.3}$$

This local volume fraction is more representative of the density of the flow for a small number of particles (even only one). In our case, the average used are either volumetric or weighted, as presented bellow.

[9] The Voronoi tesselation (or Voronoi diagram) uses the coordinates of the center of the particles and their radius to create a meshing of the space. Each Voronoi cell of the meshing represents the space "belonging" to each particle (points of space closer to the particle center than any other).

Volume average at the outlet: the quantities in the semi-circle at the outlet are calculated using a volume average of the information from the particles inside it (see fig. A.1b):

$$G = \frac{\sum_{k=1}^{n} V_k.G_k}{\sum_{k=1}^{n} V_k} \tag{A.4}$$

where G is the quantity considered (v_x, v_z,...), G_k the value for the particle k and V_k the volume of the particle inside the outlet[10]. To reduce the impact of the discrete size of the particle, we differentiate the case for a particle fully inside the outlet or partially inside (on the edge):

- For a particle fully inside the outlet (blue ones in fig. A.1b), the volume V_k is the volume of the spherical particle:

$$V_k = 4\pi r^3/3 \tag{A.5}$$

  with r the radius of the particle (in experiment, the mean radius $r = 0.55$ mm is used).

- For a particle partially inside the outlet (green ones in fig. A.1b), the volume V_k is the volume of a spherical cap created by the intersection of the particle and outlet:

$$V_k = \pi h^2(3r - h)/3 \tag{A.6}$$

$$h = r + (x_k^2 + z_k^2 - r_0) \tag{A.7}$$

  where h is the height of the cap, (x_k, z_k) the coordinates of the particle and r_0 the radius of the outlet. Note that the intersection between the edge of the outlet and the particle is always considered plane since $r_0 \gg r$.

Weighted average along the profile: the quantities for each point of the profile surrounding the outlet are calculated using a weighted average of the information from the particles close to the point (see fig. A.1c):

$$G_p = \frac{\sum_{k=1}^{n} (d - l_k).G_k}{\sum_{k=1}^{n} (d - l_k)} \tag{A.8}$$

where G_p is the value of the quantity considered at point p of the profile, $d = 1.1$ mm is the mean radius of the particle and l_k the distance between the point of the profile and the particle center. Only the particles within a distance $l_k < d$ are considered[11] (blue ones in fig. A.1c).

[10] No other weighting function is used except for the volume inside the outlet since we calculate the mean value for the entire region and not at a particular point [37].

[11] This linear weighting function was used instead of a smoother one [37] to reduce overlap due to the close proximity of each point of the profile ($\sim d$) and reduce calculation time.

References

[1] C. Hanotin, S. Kiesgen de Richter, P. Marchal, L. J. Michot, C. Baravian, Vibration-induced liquefaction of granular suspensions, Phys. Rev. Lett. 108 (2012) 198301.

[2] S. K. de Richter, G. Le Caër, R. Delannay, Heterogeneous dynamics of a granular pack under vertical tapping, EPL (Europhysics Letters) 85 (5) (2009) 58004.

[3] C. Hanotin, P. Marchal, L. J. Michot, C. Baravian, S. K. de Richter, Dynamics of vibrated granular suspensions probed by mechanical spectroscopy and diffusing wave spectroscopy measurements, Soft Matter 9 (39) (2013) 9352–9360.

[4] N. Gaudel, S. K. de Richter, N. Louvet, M. Jenny, S. Skali-Lami, Bulk and local rheology in a dense and vibrated granular suspension, Physical Review E 96 (6) (2017) 062905.

[5] P. Marchal, C. Hanotin, L. J. Michot, S. K. de Richter, Two-state model to describe the rheological behavior of vibrated granular matter, Phys. Rev. E 88 (2013) 012207.

[6] N. Gaudel, S. Kiesgen de Richter, N. Louvet, M. Jenny, S. Skali-Lami, Granular avalanches down inclined and vibrated planes, Phys. Rev. E 94 (2016) 032904.

[7] C. Hanotin, S. Kiesgen de Richter, L. Michot, P. Marchal, Viscoelasticity of vibrated granular suspensions, Journal of Rheology 59 (1) (2015) 253–273.

[8] N. Gaudel, S. Kiesgen De Richter, Effect of vibrations on granular material flows down an inclined plane using dem simulations, Powder Technology 346 (2019) 256–264.

[9] W. A. Beverloo, H. A. Leniger, J. Van de Velde, The flow of granular solids through orifices, Chemical engineering science 15 (3-4) (1961) 260–269.

[10] C. Mankoc, A. Janda, R. Arevalo, J. Pastor, I. Zuriguel, A. Garcimartín, D. Maza, The flow rate of granular materials through an orifice, Granular Matter 9 (6) (2007) 407–414.

[11] A. Janda, I. Zuriguel, D. Maza, Flow rate of particles through apertures obtained from self-similar density and velocity profiles, Physical review letters 108 (24) (2012) 248001.

[12] M. Benyamine, P. Aussillous, B. Dalloz-Dubrujeaud, Discharge flow of a granular media from a silo: effect of the packing fraction and of the hopper angle, in: EPJ Web of Conferences, Vol. 140, EDP Sciences, 2017, p. 03043.

[13] D. Höhner, S. Wirtz, V. Scherer, A study on the influence of particle shape on the mechanical interactions of granular media in a hopper using the discrete element method, Powder technology 278 (2015) 286–305.

[14] A. Anand, J. S. Curtis, C. R. Wassgren, B. C. Hancock, W. R. Ketterhagen, Predicting discharge dynamics of wet cohesive particles from a rectangular hopper using the discrete element method (dem), Chemical Engineering Science 64 (24) (2009) 5268–5275.

[15] K. To, P.-Y. Lai, H. Pak, Jamming of granular flow in a two-dimensional hopper, Physical review letters 86 (1) (2001) 71.

[16] A. Janda, I. Zuriguel, A. Garcimartín, L. A. Pugnaloni, D. Maza, Jamming and critical outlet size in the discharge of a two-dimensional silo, EPL (Europhysics Letters) 84 (4) (2008) 44002.

[17] C. Mankoc, A. Garcimartín, I. Zuriguel, D. Maza, L. A. Pugnaloni, Role of vibrations in the jamming and unjamming of grains discharging from a silo, Physical Review E 80 (1) (2009) 011309.

[18] I. Zuriguel, Á. Janda, R. Arévalo, D. Maza, Á. Garcimartín, Clogging and unclogging of many-particle systems passing through a bottleneck, in: EPJ Web of Conferences, Vol. 140, EDP Sciences, 2017, p. 01002.

[19] M. Hunt, R. Weathers, A. Lee, C. Brennen, C. Wassgren, Effects of horizontal vibration on hopper flows of granular materials, Physics of fluids 11 (1) (1999) 68–75.

[20] C. R. Wassgren, M. L. Hunt, P. Freese, J. Palamara, C. Brennen, Effects of vertical vibration on hopper flows of granular material, Physics of Fluids 14 (10) (2002) 3439–3448.

[21] A. Pascot, N. Gaudel, S. Antonyuk, J. Bianchin, S. K. De Richter, Influence of mechanical vibrations on quasi-2d silo discharge of spherical particles, Chemical Engineering Science (2020) 115749.

[22] A. Pascot, G. Marouazi, S. K. De Richter, Discharge of a granular silo under mechanical vibrations, in: EPJ Web of Conferences, Vol. 249, EDP Sciences, 2021, p. 03037.

[23] C. Goniva, C. Kloss, A. Hager, S. Pirker, An open source cfd-dem perspective, in: Proceedings of OpenFOAM Workshop, Göteborg, 2010, pp. 1–10.

[24] C. Kloss, C. Goniva, A. Hager, S. Amberger, S. Pirker, Models, algorithms and validation for opensource dem and cfd–dem, Progress in Computational Fluid Dynamics, an International Journal 12 (2-3) (2012) 140–152.

[25] P. A. Cundall, O. D. Strack, A discrete numerical model for granular assemblies, geotechnique 29 (1) (1979) 47–65.

[26] A. Di Renzo, F. P. Di Maio, An improved integral non-linear model for the contact of particles in distinct element simulations, Chemical engineering science 60 (5) (2005) 1303–1312.

[27] J. C. Crocker, D. G. Grier, Methods of digital video microscopy for colloidal studies, Journal of colloid and interface science 179 (1) (1996) 298–310.

[28] S. M. Rubio-Largo, A. Janda, D. Maza, I. Zuriguel, R. Hidalgo, Disentangling the free-fall arch paradox in silo discharge, Physical review letters 114 (23) (2015) 238002.

[29] Q. Wang, Q. Chen, R. Li, G. Zheng, R. Han, H. Yang, Shape of free-fall arch in quasi-2d silo, Particuology 55 (2021) 62–69.

[30] J. M. Pastor, A. Garcimartín, P. A. Gago, J. P. Peralta, C. Martín-Gómez, L. M. Ferrer, D. Maza, D. R. Parisi, L. A. Pugnaloni, I. Zuriguel, Experimental proof of faster-is-slower in systems of frictional particles flowing through constrictions, Physical Review E 92 (6) (2015) 062817.

[31] A. Goldshtein, M. Shapiro, L. Moldavsky, M. Fichman, Mechanics of collisional motion of granular materials. part 2. wave propagation through vibrofluidized granular layers, Journal of Fluid Mechanics 287 (1995) 349–382.

[32] J. Bougie, S. J. Moon, J. Swift, H. L. Swinney, Shocks in vertically oscillated granular layers, Physical Review E 66 (5) (2002) 051301.

[33] R. Nedderman, U. Tüzün, A kinematic model for the flow of granular materials, Powder Technology 22 (2) (1979) 243–253.

[34] A. Medina, J. Cordova, E. Luna, C. Trevino, Velocity field measurements in granular gravity flow in a near 2d silo, Physics Letters A 250 (1-3) (1998) 111–116.

[35] J. Choi, A. Kudrolli, M. Z. Bazant, Velocity profile of granular flows inside silos and hoppers, Journal of Physics: Condensed Matter 17 (24) (2005) S2533.

[36] B. Glasser, I. Goldhirsch, Scale dependence, correlations, and fluctuations of stresses in rapid granular flows, Physics of Fluids 13 (2) (2001) 407–420.

[37] H. Zhu, A. Yu, Averaging method of granular materials, Physical Review E 66 (2) (2002) 021302.

[38] K. A. Alshibli, H. A. El-Saidany, Quantifying void ratio in granular materials using voronoi tessellation, Journal of computing in civil engineering 15 (3) (2001) 232–238.

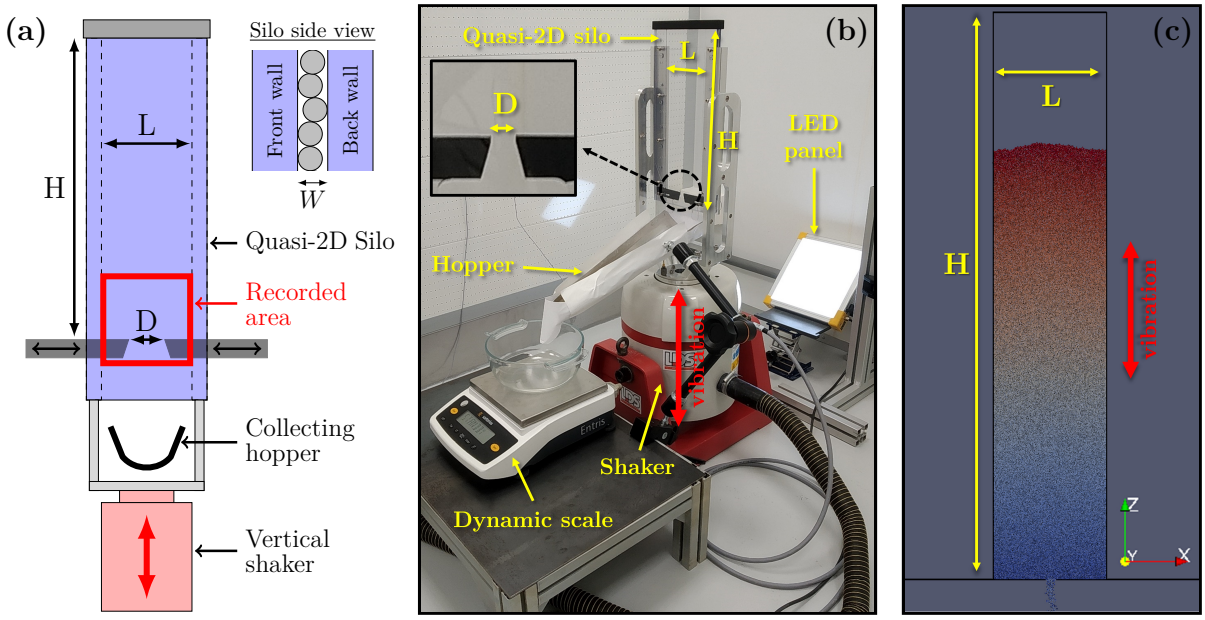

Figure 1: (a) Schematic diagram of the experimental setup: front view of the silo mounted on the shaker and side view of the "quasi-2D" aspect (the grey spheres represent the particles). (b) Side view of the experimental setup and close-up of the opening ($D = 10.41$ mm on the picture). (c) Snapshot of the simulated system with the same geometry as the experiment. Particles are colored in order of insertion, from blue to red.

Parameter	Value/Range
H (silo height)	300 mm
L (silo width)	100 mm
W (silo depth)	1.5 mm
D (silo opening)	$4.99 - 21.53$ mm
d (particle diameter)	1.1 ± 0.1 mm
ρ (particle density)	2500 kg/m^3
A (vibration amplitude)	$0 - 2800$ µm
f (vibration frequency)	15-75 Hz

Table 1: Properties for the silo geometry, particles and vibrations used in experiment

Parameter	Value
N (number of particle)	40 000
E (Young modulus)	5×10^6 Pa
ν (Poisson coefficient)	0.22
e_{pp} | e_{pw} (restitution coefficients)	0.97 | 0.83
μ_{pp} | μ_{pw} (friction coefficients)	0.4 | 0.15

Table 2: Particle properties used in the simulation. The subscripts pp and pw indicate particle-particle and particle-wall contact properties, respectively.

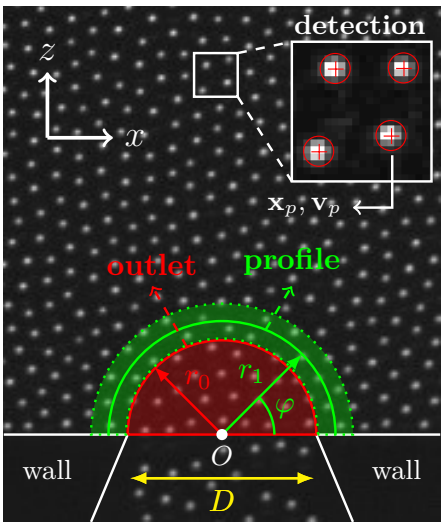

Figure 2: Close-up of the silo opening in experiment, with the particle centers appearing as bright spots that can be tracked during the discharge. In the referential of the silo, the origin O is set in the middle of the silo opening. The information on the flow are measured in the outlet region (semicircle colored in red, $r_0 = D/2$) and along a surrounding radial profile (line in green, $r_1 = D/2 + d$) with a thickness $2d$ (colored in green) to avoid discrete effects due to particle size.

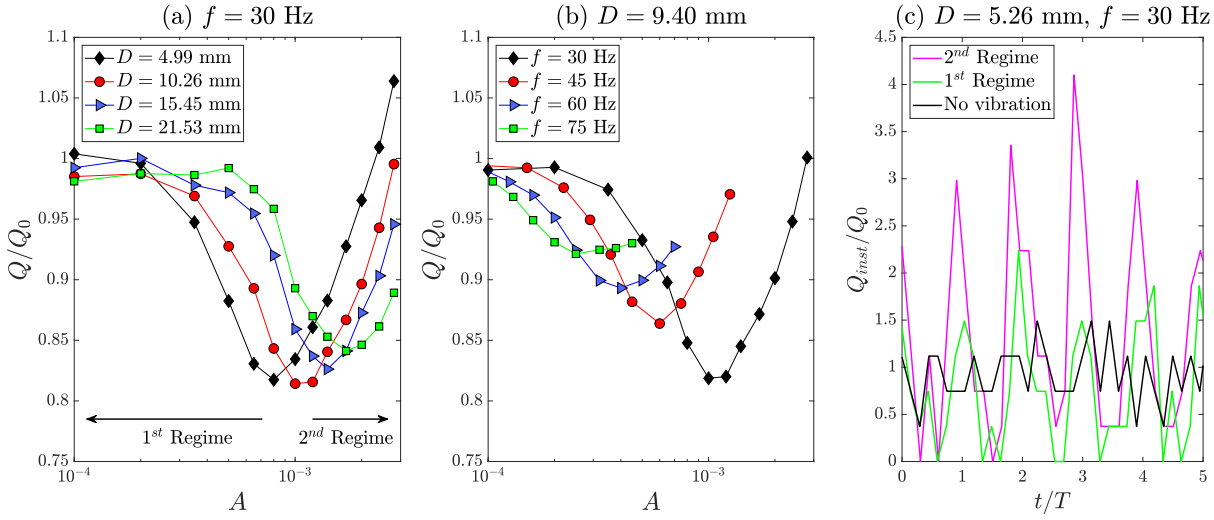

Figure 3: Evolution of the normalized flow rate Q/Q_0 (with Q_0 the flow rate without vibration) as a function of the vibration amplitude A in experiment for (a) different opening sizes D (vibration frequency $f = 30$ Hz) and (b) different frequencies f (opening size $D = 9.41$ mm). Two different regimes are observed for the flow rate depending on the amplitude, opening size and frequency. (c) Typical normalized instantaneous flow rate Q_{inst}/Q_0 (flow rate measured over an interval $\Delta t = 0.005$ s) during the discharge measured in experiment without vibration and in each regime (with $T = 1/f$ the period of vibration).

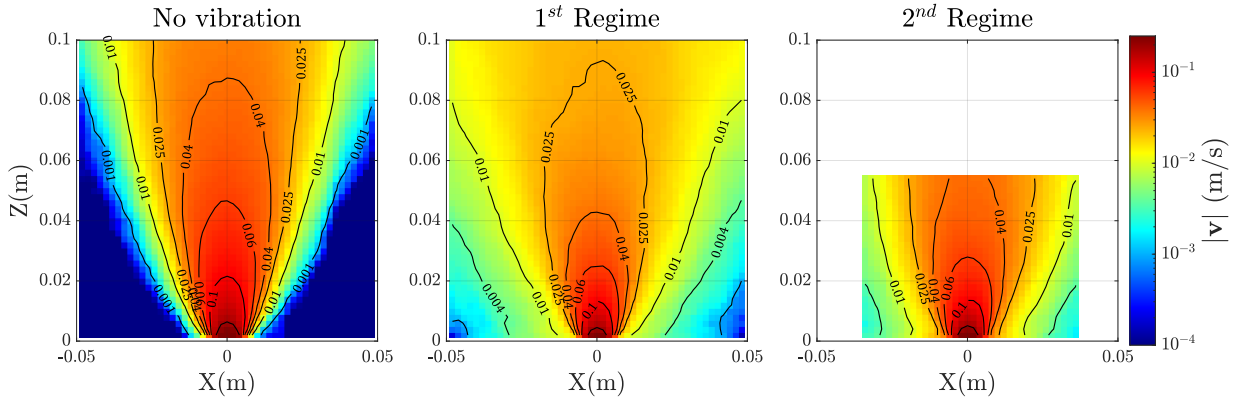

Figure 4: Typical mean velocity field $|\mathbf{v}|$ near the silo opening obtained in each regime in experiment (vibration frequency $f = 30$ Hz and an opening size $D = 10.26$ mm). Due to higher vibration velocities in the second regime, the recorded area was limited to ensure a sufficient recording frequency (2000 images/s) for the particle tracking.

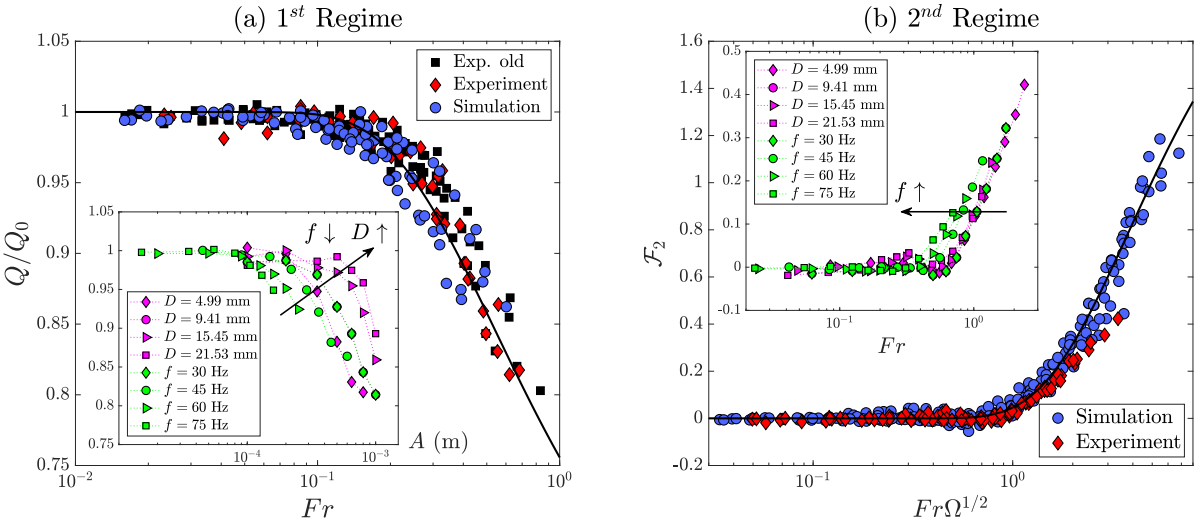

Figure 5: (a) Dimensionless flow rate Q/Q_0 as a function of the Froude number Fr for all cases in experiment and simulation (including previous results from the literature [21], noted "Exp. old"). Data are fitted to $1+\mathcal{F}_1$ (see eq. 5), with $a_1 = 0.420$ and $b_1 = 0.542$ ($R^2 = 908$). Insert: Raw data showing the evolution of the normalised flow rate as a function of the amplitude of vibration A for different opening sizes D (in magenta with $f = 30$ Hz) and frequencies $f = 30 - 75$ Hz (in green with $D = 9.41$ mm). (b) Dimensionless flow rate $\mathcal{F}_2$ as a function of $Fr\Omega^{1/2}$ for both experiments and simulations. Data are fitted to $\mathcal{F}_2$ (see eq. 7), with $a_2 = 2.18$ and $b_2 = 3.86$ ($R^2 = 0.985$). Insert: $\mathcal{F}_2$ as a function of Fr number for different opening sizes D (in magenta with $f = 30$ Hz) and frequencies $f = 30 - 75$ Hz (in green with $D = 9.41$ mm).

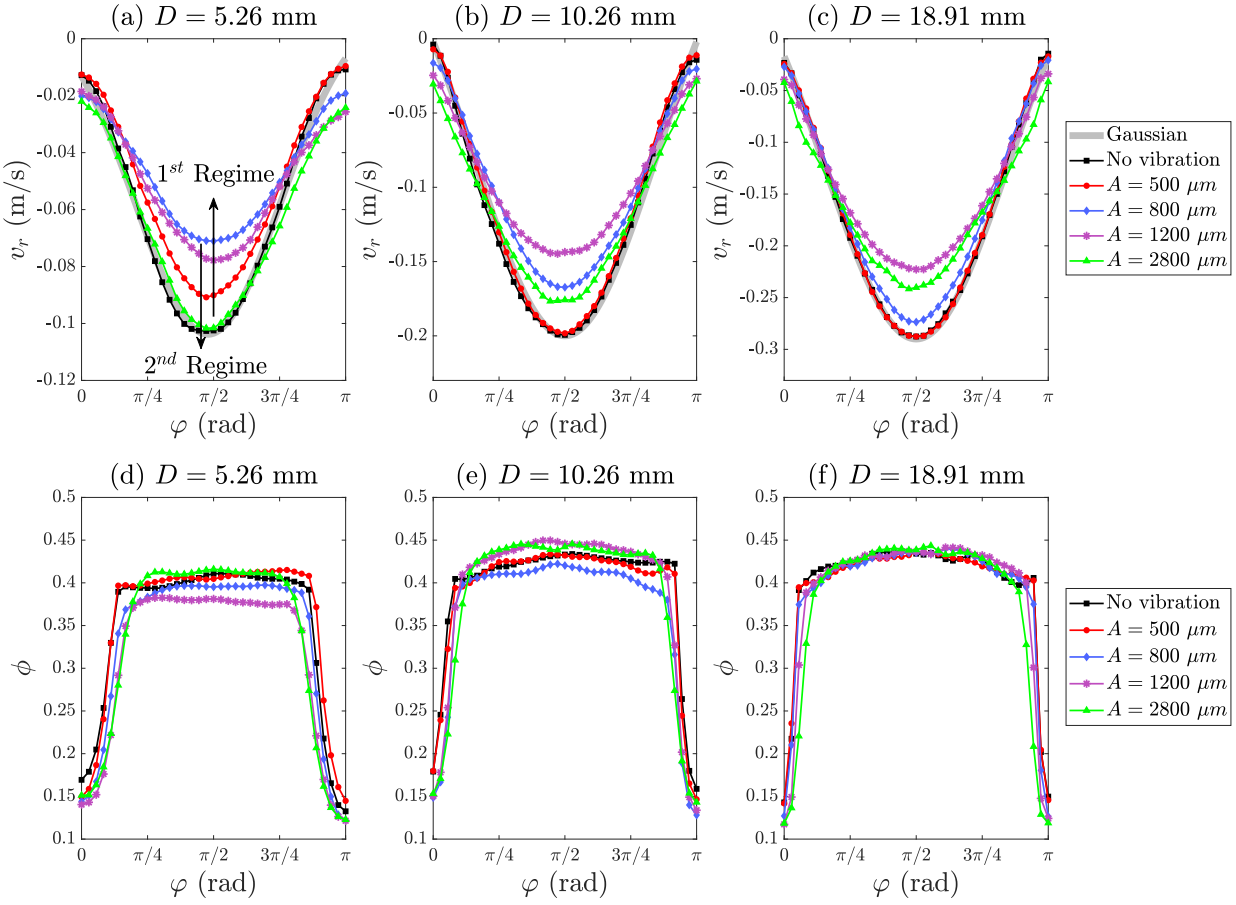

Figure 6: Profiles of the radial velocity v_r (a,b,c) and volume fraction ϕ (d,e,f) along the radial profile surrounding the outlet in experiment for different opening sizes $D = 5.26 - 18.91$ mm and amplitudes $A = 0 - 2800$ µm ($f = 30$ Hz). Without vibration, the velocity profile is Gaussian (grey solid line).

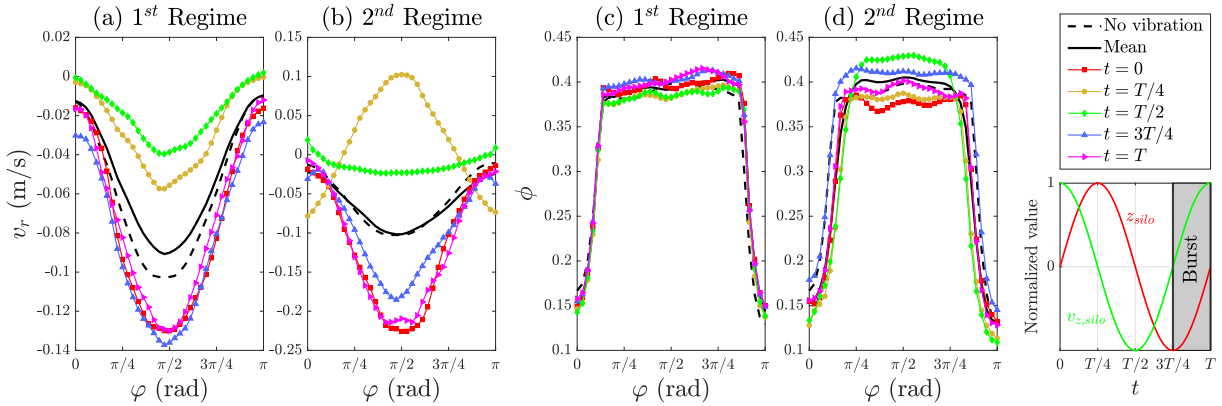

Figure 7: Experimental profiles of radial velocity v_r (a,b) and volume fraction ϕ (c,d) in the first ($A = 500$ µm) and second regime ($A = 2800$ µm) at different times during a period of vibration T ($D = 5.26$ mm, $f = 30$ Hz). In each case, the profiles are time averaged over 60 periods of vibration. The bursts of velocity are observed between $3T/4$ and T, when the silo starts to go up while the particles fall down as shown in the diagram bellow the legend. The volume fraction transiently increases in the center of the funnel, leading to a compression wave of the particles which are ejected from the opening.

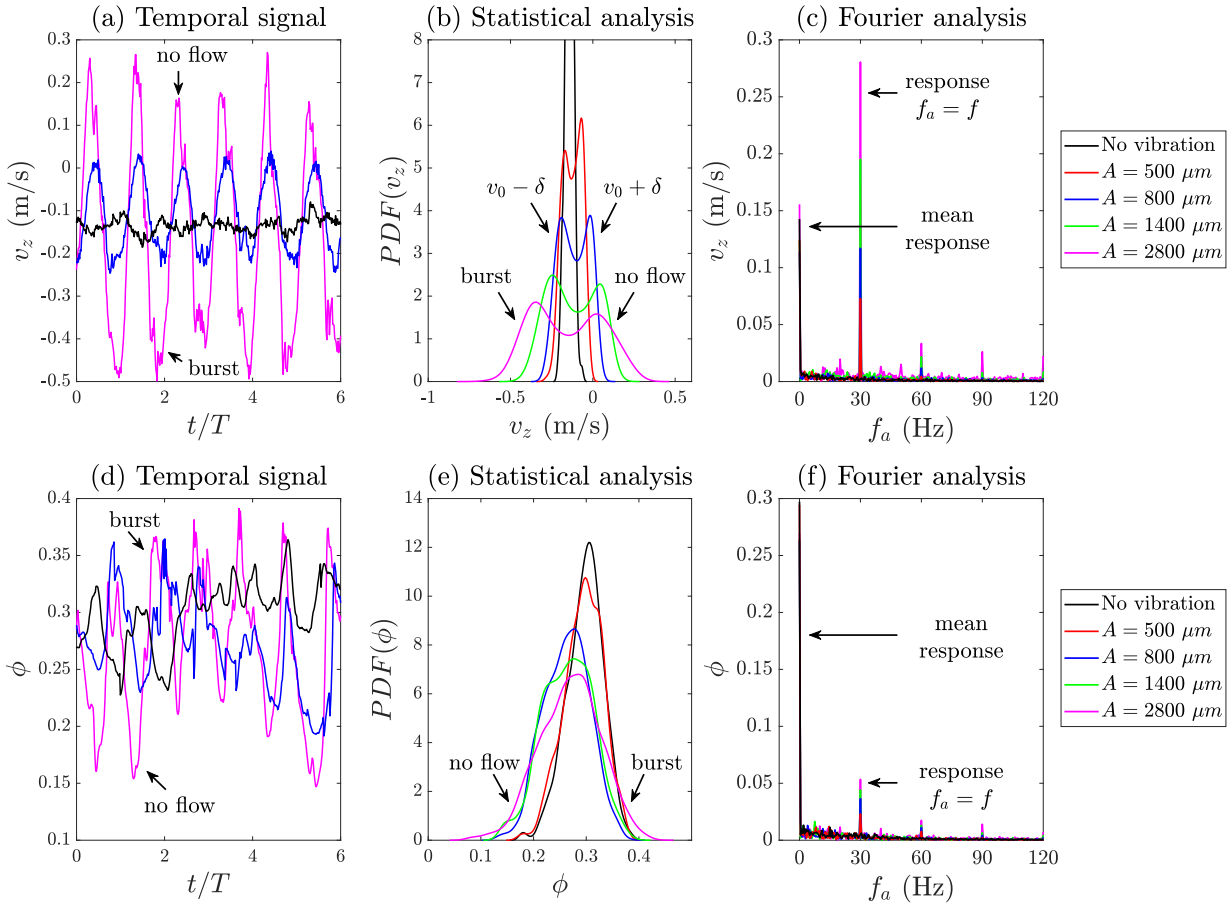

Figure 8: Experimental time evolution, probability density function (PDF), Fourier analysis of the vertical velocity v_z (a,b,c) at the outlet and volume fraction ϕ (d,e,f) for various amplitudes $A = 0 - 2800$ µm ($f = 30$ Hz, $D = 5.26$ mm). Periodic fluctuations ($\pm\delta$) can be observed in the first regime ($A = 500 - 800$ µm). The period of the fluctuations is the same as the one for vibrations T. In the second regime ($A = 1400 - 2800$ µm), an oscillation between two states ("burst" of flow rate and nearly "no flow") is observed due to the shock dynamics. In addition to the mean response (at $f_a = 0$ Hz), this leads to an harmonic response with the vibration (at $f_a = f$).

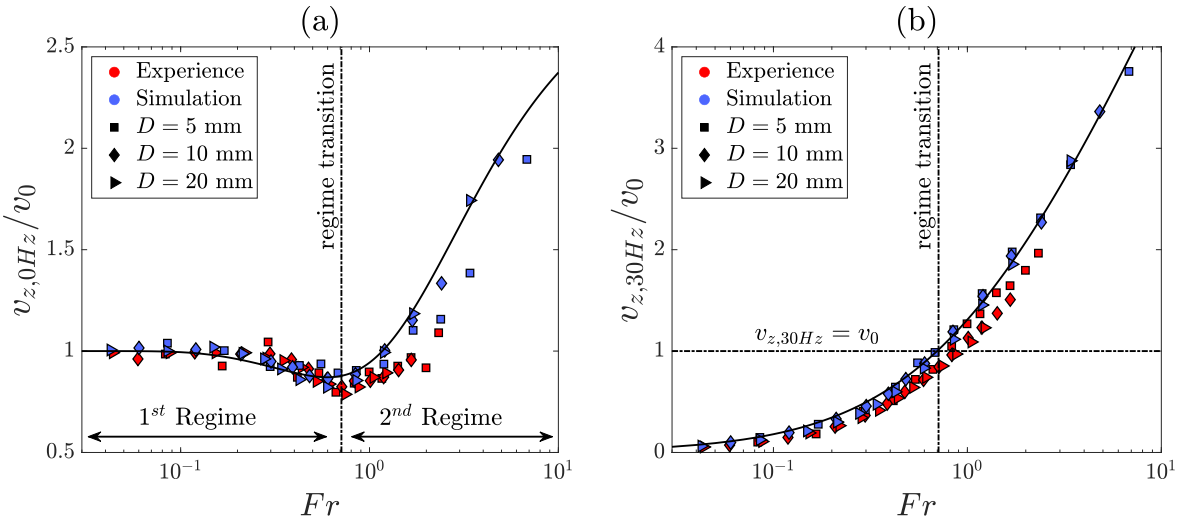

Figure 9: Dimensionless (a) mean response $v_{z,0Hz}/v_0$ and (b) response at the vibration frequency $v_{z,30Hz}/v_0$ as function of the Froude number Fr for different opening size D in experiment and simulation. The mean response is well described by the empirical law for the flow rate 8 while the response at f increases with the Froude number (see eq. 12). The regime transition occurs for $v_{z,30Hz} = v_0$, switching from a steady regime with small perturbations to a completely vibration driven regime.

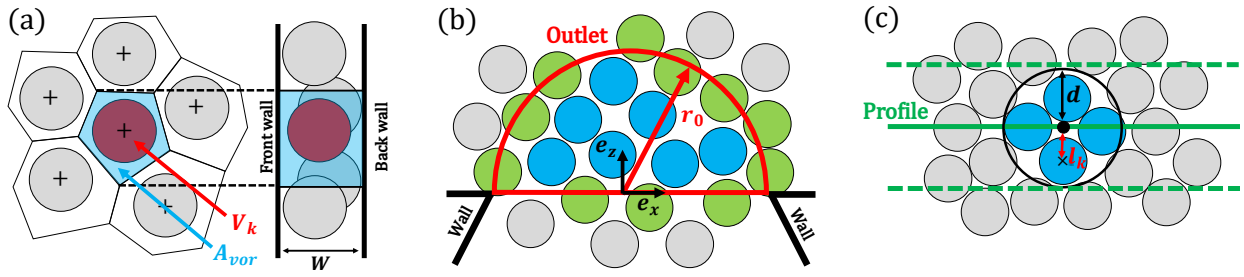

Figure A.1: Methods used to calculate the velocity and volume fraction in the silo. (a) Front and side view of the 2D Voronoi tessellation around a few particles in the silo (colored in gray and red). The Voronoi volume V_{vor} belonging to the red particle (colored in blue) is equal to the area A_{vor} times the depth of the silo W. (b) Particles used to calculate the quantities at the outlet (red semi-circle of radius $r_0 = D/2$) using the volume average (eq. A.1): the particles colored in blue are fully inside the outlet while the ones in green are partially inside. For the latter, only the volume of the cap formed by the intersection between the particle and outlet edge is considered. (c) Particles used to calculate the quantities at one point of the profile around the outlet (radial profile of radius $r_1 = D/2 + d$) using the weighted average (eq. A.4): only the particles whose center is at a distance $l_k < d$ from the point are considered (colored in blue).

Discharge of vibrated granular silo: a grain scale approach

Powder Technology

Methods

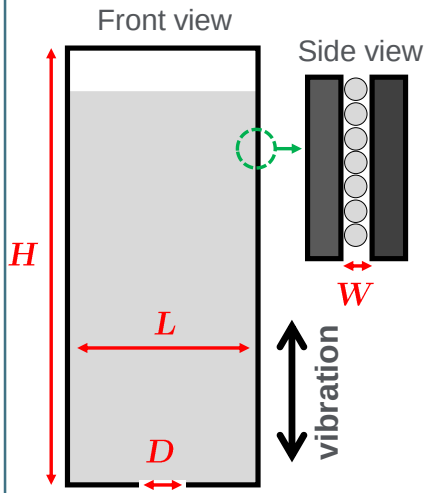

- Quasi-2D granular silo under vibrations
- Discharge of spherical glass beads (diameter $d \sim 1$ mm, density ρ)
- Controlled vertical sinusoidal vibration
- Experiments + DEM simulations for varying opening & vibration

Results:

- Two flow regimes with vibration
- Competition between vibration and gravity
- Depends on Froude number + relative frequency
- 1st regime: vib. ≤ gravity, 2nd regime: vib. > gravity
- Effect purely on velocity (constant volume fraction)

Conclusion: Flow rate law under vibration:

$$Q = \rho \phi_0 W D \mathcal{V}_{vib} \quad , \quad \mathcal{V}_{vib} = C\sqrt{gD}(1 + \mathcal{F}_1 + \mathcal{F}_2)$$

Volume fraction at silo outlet

No vibration

- Funnel flow, gravity driven
- Negligible time fluctuations, large dead zones

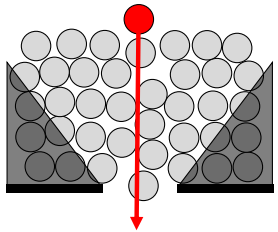

1st Regime

- Mass flow, gravity + vibration driven
- ↑ Fluctuations, ↑ contacts, ↓ dead zones
- ↓ **Flow rate**

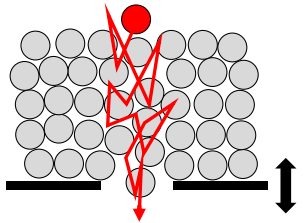

2nd Regime

- Shock dynamic, vibration driven
- ↑↑ Fluctuations, ↓ Dead zones
- ↑↑ **Flow rate**

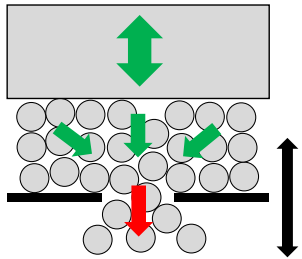

Pascot et al. 2021